Planar density-functional approach to the solid-fluid interface of simple liquids

D. W. Marr and A. P. Gast

Department of Chemical Engineering, Stanford University, Stanford, California 94305-5025

A planar formulation of the weighted-density approximation is applied to the solid-fluid interface of simple liquids. Computational requirements are reduced from the previous theory through definition of a one-dimensional weighted density that recognizes the planar symmetry of the interface. After finding good agreement with hard-sphere Monte Carlo results, the approach is extended to attractive systems, in particular, the Lennard-Jones fluid. This system provides a stringent test of the model due to its long-range interactions; it is a well-studied example of systems whose density difference varies with temperature. Interfacial tensions are determined for both the solid-liquid and solid-vapor regions of the phase diagram, and reasonable agreement is found with molecular-dynamics simulations at the triple point.

PACS number(s): 68.45.Ws, 82.65.Dp

I. INTRODUCTION

Since the first simulations of the hard-sphere, fluid-solid transition in 1968 [1, 2], there has been tremendous interest in entropically driven freezing processes. Despite this activity, successful analytic descriptions of hard-sphere crystallization have remained elusive. Recently, density-functional theory has provided a means to describe the structure, energetics, and phase coexistence of the hard-sphere solid. In addition to its facility with the hard-sphere fluid-solid transition, density-functional theory has allowed description of interfaces and other inhomogeneous systems through the principles of liquid-state theory. In this paper we present a tractable approach to the hard-sphere fluid-solid interface and apply this approach to a model system of Lennard-Jones particles.

While there are a number of implementations of density-functional theory for studying phase transitions, all of them seek to describe the structure and properties of the solid phase by using information known about the fluid. Several excellent reviews of the different density-functional approaches have recently appeared [3–8]. In one such approach, Curtin and Ashcroft [9] define a weighting function which links the solid and liquid states. This approach, known as the weighted-density approximation (WDA), involves the determination of a spatially *variant* weighted density where fluid properties approximate those of the solid. This method has been effective in predicting solid properties and phase coexistence, but its application to more complex problems has been hindered by the computational requirements in the determination of weighted densities. To overcome these difficulties, Denton and Ashcroft have developed the modified weighted-density approximation (MWDA) [10]. In contrast to the WDA, this approach requires only calculation of a spatially *invariant* weighted density and significantly lowers computation time. Hard-sphere fluid-solid results for the WDA and MWDA agree quite well with Monte Carlo calculations [2].

In order to study the structural details and energetics of the solid-liquid interface, one must determine the appropriate weighted density to model each density through the interface. This can be done with the WDA [11, 12]; however, the calculation requires tremendous computational effort making it impractical for complex situations. We are interested in systems including finite interparticle interactions where the densities of coexisting phases will depend on temperature. In this situation, the interfacial structure and energy must be determined for a variety of temperatures, significantly increasing the required amount of computation and motivating us to develop a tractable approach to describe the interface. Encouraged by the success of the MWDA in decreasing the computational requirements of the WDA, we introduce a planar weighted-density approximation (PWDA) to describe the interface. Recognizing that the average density is *invariant* along the plane of the interface, we reduce computational requirements by averaging within the plane in the same manner as the MWDA. Before introducing this approach we first review the WDA and MWDA. We then apply the PWDA first to the bulk fluid-solid transition and then to the hard-sphere interface. Finally, we apply the PWDA to a model system whose coexisting densities vary with temperature in a description of the fluid-solid interface for Lennard-Jones molecules.

II. DENSITY-FUNCTIONAL THEORY

We begin by separating the total Helmholtz free energy of the solid phase into three components

$$F[\rho] = F_{\text{id}}[\rho] + F_{\text{ex}}[\rho] + F_{\text{ext}}[\rho] \qquad (1)$$

representing the ideal, excess, and external field contributions to the total free energy. Henceforth, we set the external field contribution to zero. The ideal term can be calculated for any given density distribution $\rho(\mathbf{r})$ from

$$F_{\text{id}}[\rho] = \beta^{-1} \int d\mathbf{r} \rho(\mathbf{r}) \{ \ln[\rho(\mathbf{r})\Lambda^3] - 1 \}, \qquad (2)$$

where $\beta = 1/kT$ and Λ is the deBroglie wavelength, and the total excess free energy can be expressed as the sum of local contributions

$$F_{\rm ex}[\rho] = \int d\mathbf{r}\rho(\mathbf{r})\psi(\mathbf{r};[\rho]), \tag{3}$$

where ψ is the local excess free energy per particle.

A. Weighted-density approximation

Following Curtin and Ashcroft [9], we then approximate the local excess solid free energy per particle with the excess free energy per particle of a homogeneous fluid evaluated at some effective liquid density $\bar{\rho}$,

$$F_{\rm ex}^{\rm WDA}[\rho] \equiv \int d\mathbf{r}\rho(\mathbf{r})\psi_0(\bar{\rho}(\mathbf{r})) \tag{4}$$

where the effective liquid density is a weighted average of the local solid densities in the vicinity of $\mathbf{r}$. In the WDA, the spatially *variant* effective liquid density is defined by

$$\bar{\rho}(\mathbf{r}) \equiv \int d\mathbf{r}'\rho(\mathbf{r}')w(\mathbf{r} - \mathbf{r}';\bar{\rho}(\mathbf{r})), \tag{5}$$

where the weighting function w has been introduced with the normalization requirement

$$\int d\mathbf{r}w(\mathbf{r} - \mathbf{r}';\rho) = 1 \tag{6}$$

and is determined by requiring the exact two-particle direct correlation function to be recovered in the homogeneous limit indicated by a subscript 0,

$$-\beta^{-1}c_0(\mathbf{r} - \mathbf{r}';\rho_0) = \lim_{\rho\to\rho_0}\frac{\delta^2 F_{\rm ex}}{\delta\rho(\mathbf{r})\delta\rho(\mathbf{r}')}. \tag{7}$$

Solving for w is most readily done in Fourier space, leading to the following differential equation where derivatives are taken with respect to density and the free energies are evaluated at ρ_0

$$-\beta^{-1}c_0(k;\rho_0) = 2\psi_0'w(k;\rho_0) + \rho_0\frac{\partial}{\partial\rho_0}\left[\psi_0'w^2(k;\rho_0)\right]. \tag{8}$$

This equation satisfies the compressibility equation, re-

ducing in the $k = 0$ case to

$$-\beta^{-1}c_0(k = 0;\rho_0) = 2\psi_0' + \rho_0\psi_0''. \tag{9}$$

B. Modified weighted-density approximation

The MWDA [10] differs from this approach in that the excess Helmholtz free energy is calculated from a spatially invariant weighted density

$$F_{\rm ex}^{\rm MWDA}[\rho] \equiv N\psi_0(\hat{\rho}), \tag{10}$$

where N is the number of particles and with the weighted density determined from

$$\hat{\rho} \equiv \frac{1}{N}\int d\mathbf{r}\rho(\mathbf{r})\int d\mathbf{r}'\rho(\mathbf{r}')w(\mathbf{r} - \mathbf{r}';\hat{\rho}). \tag{11}$$

Using the normalization condition on w [Eq. (6)] and imposing the exact fluid free energy in the homogeneous limit [Eq. (7)] we obtain for w

$$-\beta^{-1}c_0(k;\rho_0) = 2\psi_0'w(k;\rho_0) + \delta_{k,0}\rho_0\psi_0''. \tag{12}$$

This equation for $w(k,\rho)$ is easier to solve than the WDA, being proportional to the direct correlation function (for nonzero k) and not involving the solution of a nonlinear differential equation. Both the WDA and the MWDA compare favorably with Monte Carlo results for hard spheres (see Table I), but the MWDA requires a great deal less computation and is therefore the preferred approach for the study of the transition from liquid to solid [3, 7, 8, 13–17].

C. Planar weighted-density approximation

In systems such as the solid-fluid interface where the bulk density varies with position, one cannot apply the MWDA because of the need for a spatially varying weighted density. Curtin [12] has applied the WDA to the interfacial problem with good results but with significant computational effort. We have attempted to lower these requirements while still retaining the physical approach to the problem by incorporating the MWDA into the interface. This is done by realizing that the bulk density parallel to a planar interface remains constant. In

TABLE I. Comparison of various theories for hard-sphere phase coexistence [L is the Lindemann parameter, $(3/\alpha a^2)^{1/2}$], including molecular dynamics (MD), Monte Carlo calculations (MC), the effective liquid approximation (ELA), the self-consistent ELA (SCELA), and the generalized ELA (GELA).

	Fluid density $\rho_f\sigma^3$	Solid density $\rho_s\sigma^3$	Density difference $\Delta\rho\sigma^3$	Pressure $\beta P\sigma^3$	L
MD [1]	0.949	1.048	0.098	12.1	
MC [2]	0.943	1.041	0.097	11.7	0.126
GELA [29]	0.945	1.041	0.095	11.9	0.100
SCELA [29]	0.970	1.070	0.099	13.3	0.084
ELA [30]	0.993	1.083	0.090	16.1	0.074
WDA [9, 12]	0.881	1.02	0.139	9.5	0.101
MWDA [10, 31]	0.912	1.044	0.132	10.1	0.097
PWDA (this work)	0.882	1.026	0.144	9.5	0.100

the spirit of Denton and Ashcroft's approach to lowering the computational requirements for WDA models of bulk systems, we will approach the interface with a planar-averaged spatially variant weighted density that will significantly decrease calculation costs. Other authors have succeeded in modeling systems such as a hard-sphere fluid next to a hard wall [18–20] with a one-dimensional weighted density; however, efforts to describe the freezing transition with such a weighted density have not, to date, led to a stable solid. We begin by expressing the excess free energy in terms of the planar-averaged density $\hat{\rho}(z)$ and a planar-averaged free energy

$$F_{\text{ex}}[\rho] = \int d\mathbf{r} \hat{\rho}(z)\psi(z),\tag{13}$$

$$\hat{\rho}(z) = \frac{1}{A}\int dx\, dy\, \rho(\mathbf{r}).\tag{14}$$

We now approximate this "local" free energy with that of a homogeneous fluid evaluated at the planar weighted density $\overline{\rho}(z)$

$$F_{\text{ex}}^{\text{PWDA}}[\rho] \equiv \int d\mathbf{r} \hat{\rho}(z)\psi_0(\overline{\rho}(z)),\tag{15}$$

determined self-consistently from

$$\overline{\rho}(z) \equiv \frac{\int dx\, dy\, \rho(\mathbf{r}) \int d\mathbf{r}' \rho(\mathbf{r}') w(\mathbf{r} - \mathbf{r}'; \overline{\rho}(z))}{\int dx\, dy\, \rho(\mathbf{r})}\tag{16}$$

where once again the weighting function is determined from the normalization condition [Eq. (6)] and the requirement on the limiting behavior [Eq. (7)]. In Fourier space we obtain

$$\begin{aligned}-\beta^{-1}c_0(k;\rho_0) = {}&2\psi_0' w(k;\rho_0)\\&+ \delta_{\mathbf{k}_{||},0}\rho_0\frac{\partial}{\partial\rho_0}\left[\psi_0' w^2(k;\rho_0)\right],\end{aligned}\tag{17}$$

an expression obeying the compressibility equation [Eq. (9)] and reducing in the $\mathbf{k}_{||} = 0$ case to the WDA weighting function. When $\mathbf{k}_{||}$ is nonzero we obtain the MWDA weighting function.

III. THE BULK FLUID-SOLID TRANSITION

In order to solve these equations for the solid free energy we must first model the solid structure. As originally proposed by Tarazona [21], we assume that the solid is an fcc lattice with a density distribution represented as the sum of normalized Gaussians

$$\rho_s(\mathbf{r}) = \left(\frac{\alpha}{\pi}\right)^{3/2}\sum_{\mathbf{R}} e^{-\alpha(\mathbf{r}-\mathbf{R})^2},\tag{18a}$$

where $\mathbf{R}$ are the Bravais lattice vectors for an fcc lattice, or in Fourier space as

$$\rho_s(\mathbf{r}) = \rho_s + \sum_{\mathbf{G}\neq 0}\rho_G e^{i\mathbf{G}\cdot\mathbf{r}},\tag{18b}$$

where $\mathbf{G}$ are the reciprocal lattice vectors for an fcc lattice and $\rho_G \equiv \rho_s e^{-G^2/4\alpha}$. The parameter α describes the structure of the solid; the higher the value of α, the more localized the structure and a value of zero corresponds

to the homogeneous fluid. We calculate both $\psi_0(\rho)$ and $c_0(k;\rho)$ with the Percus-Yevick approximation [10] allowing determination of the solid excess free energy for a given α and bulk solid density ρ_s. The procedure we follow is to minimize the total free energy for a given solid density with respect to α. A global minimum occurring at a nonzero α indicates a stable solid phase. We therefore determine both the stable α and excess free energy corresponding to a given solid density. The total free energy is found by adding the ideal and excess contributions. Phase coexistence occurs when the chemical potential μ and pressure P of the solid and fluid phases are identical:

$$\mu = \frac{\partial(\rho\frac{F[\rho]}{N})}{\partial\rho},\tag{19}$$

$$P = \rho(\mu - F[\rho]/N) = \rho^2\frac{\partial(\frac{F[\rho]}{N})}{\partial\rho}.\tag{20}$$

The results of these calculations for the WDA, the MWDA, and the PWDA are shown in Table I along with results from simulation and several other versions of density-functional theory.

IV. THE INTERFACE

A. Interfacial tension

In order to determine interfacial properties we first calculate bulk properties including the pressure, chemical potential, solid localization parameter, and the densities of the coexisting bulk phases following Sec. III. While μ and P remain constant throughout the interface, the coexisting densities define the boundary conditions on the interfacial profile. We then determine both interfacial structure (width) and interfacial energy (surface tension) by minimizing the excess grand potential $\Delta\Omega$

$$\Delta\Omega[\rho(\mathbf{r})] = F[\rho(\mathbf{r})] - \mu\int d\mathbf{r}\rho(\mathbf{r}) + PV.\tag{21}$$

Applying Eqs. (1) and (2) and the PWDA we obtain

$$\begin{aligned}\Delta\Omega[\rho(\mathbf{r})] = {}&F_{\text{ex}}^{\text{PWDA}}[\rho(\mathbf{r})] + PV\\&+ \int d\mathbf{r}\rho(\mathbf{r})[\beta^{-1}\{\ln[\rho(\mathbf{r})\Lambda^3] - 1\} - \mu].\end{aligned}\tag{22}$$

Finally, after applying Eq. (15) and making the following definitions

$$\hat{f}_{\text{id}}(z) = \frac{1}{A}\int dx\, dy\, \rho(\mathbf{r})\ln\rho(\mathbf{r}),\tag{23}$$

$$\hat{\mu} = \beta\mu - (\ln\Lambda^3 - 1)\tag{24}$$

we obtain

$$\frac{\beta\Delta\Omega}{A} = \int dz\{\hat{\rho}(z)[\beta\psi_0(\overline{\rho}(z)) - \hat{\mu}] + \hat{f}_{\text{id}}(z) + \beta P\}.\tag{25}$$

We now minimize $\Delta\Omega$ with respect to the interfacial width subject to the limiting conditions on the bulk den-

sities at either side of the interface. This provides the interfacial tension as

$$\gamma = \frac{\Delta\Omega}{A}\bigg|_{\min}. \tag{26}$$

B. Density parametrization

To model the interface we follow Curtin [11, 12] in his application of the WDA to the hard-sphere interface. We represent the solid as the sum of Fourier components as before, but now allow these components to decay as we make the transition from solid to liquid along the z direction across the interface:

$$\rho(\mathbf{r}) = \rho_l + (\rho_s - \rho_l)f_0(z) + \sum_G \rho_G f_G(z)e^{i\mathbf{G}\cdot\mathbf{r}}, \tag{27}$$

where

$$f_G(z) = \begin{cases} 1, & |z| < z_0 \\ \frac{1}{2}[1 + \cos(\pi\frac{z-z_0}{\Delta z_G})], & z_0 < |z| < z_G \\ 0, & z_G < |z| \end{cases} \tag{28}$$

and z_0 is the position of the solid-fluid interface boundary, Δz the interface width, $f_0(z) = f_{G_1}(z)$, and $\Delta z_G = (G_1/G)^\nu \Delta z = z_G - z_0$. While Eq. (28) actually corresponds to a slab geometry, z_0 is large enough to accurately represent bulk solid properties within the slab. The decay rate of the higher-order Fourier components is described by ν and will be set equal to 0.25, the value shown to provide the minimum free energy for the hard-sphere interface [12]. Figure 1 shows an example of this
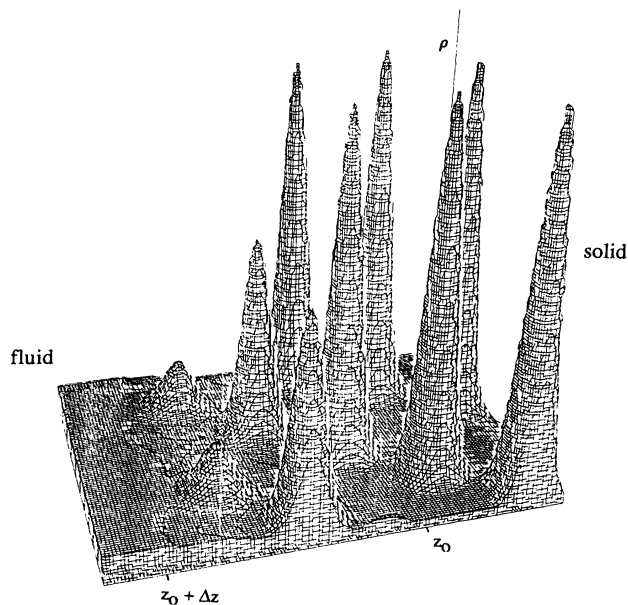

FIG. 1. Interfacial profile for $\Delta z/\delta = 3$, $\rho_s\sigma^3 = 1.0$, $\rho_l\sigma^3 = 0.9$, $\alpha\sigma^2 = 20$. A low value of α was chosen to better illustrate the transition from liquid to solid.

interfacial profile parametrization. We can now express the weighted density in the WDA in terms of the reciprocal lattice vectors and the Fourier transforms $w(k; \rho)$ and $f_G(k)$:

$$\bar{\rho}(\mathbf{r}) = \rho_l + (\rho_s - \rho_l)\frac{1}{2\pi}\int dk e^{-ikz}w(k_z; \bar{\rho}(\mathbf{r}))f_0(-k) + \frac{\rho_s}{2\pi}\sum_G e^{[i(G_x x + G_y y) - G^2/4\alpha]}$$

$$\times \int dk e^{-ikz}w((G_x^2 + G_y^2 + k^2)^{1/2}; \bar{\rho}(\mathbf{r}))f_G(k + G_z). \tag{29}$$

A similar expression has been developed for the PWDA in terms of this density parametrization and is presented in Appendix A along with some calculational details.

C. Hard-sphere results

We choose to study the interface along the densest face (111) of the close-packed fcc array, and define the z direction $\perp$ to it. We normalize z with the distance between planes, $\delta = a/\sqrt{3}$, a being the fcc lattice constant equal to $(4/\rho_s)^{1/3}$. We see excellent agreement between the PWDA and both the WDA and the MWDA in a calculation of the hard-sphere order-disorder transition (see Table I). All three of the theories agree reasonably well with Monte Carlo simulations, justifying their use in describing the hard-sphere system.

There exist few studies of the hard-sphere interface; however, we compare results from the planar-averaged approach to those obtained using the fully

three-dimensional WDA in Fig. 2. We find that the two theories agree extremely well with $\gamma^{\text{WDA}}\sigma^2/kT = 0.63 \pm 0.02$, $\Delta z^{\text{WDA}}/\delta = 3 - 4$ and $\gamma^{\text{PWDA}}\sigma^2/kT = 0.60 \pm 0.02$, $\Delta z^{\text{PWDA}}/\delta = 3 - 4$. The interfacial tension and thicknesses determined from the PWDA are equivalent to those from the WDA within computational error described in detail in Appendix B.

D. The Lennard-Jones fluid

We wish to extend the treatment of the interface to include solidification in systems having attractive interactions such as those modeled with the Lennard-Jones potential:

$$\phi_{lj}(r) = \frac{4}{T^*}\left[\left(\frac{\sigma}{r}\right)^{12} - \left(\frac{\sigma}{r}\right)^6\right], \tag{30}$$

where $T^* = kT/\varepsilon$, ε is the attractive well depth, and σ the distance r where the potential equals zero.
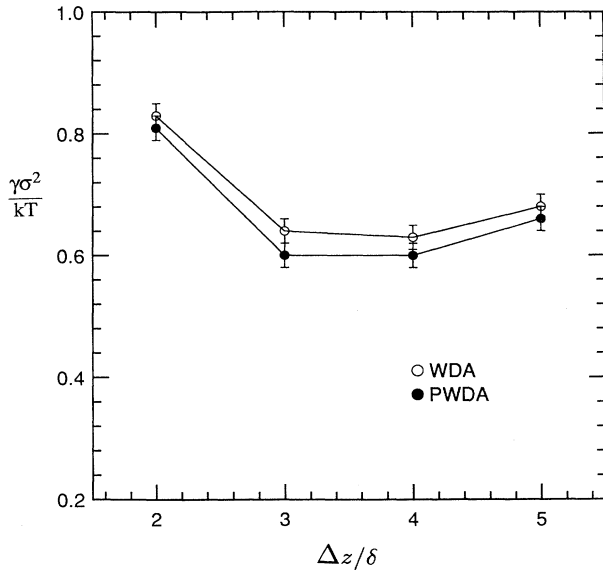
FIG. 2. Comparison of calculated hard-sphere interfacial tensions vs interfacial width between PWDA and WDA [12] theories ($\nu = 0.25$).

We follow Barker-Henderson perturbation theory [22] separating the potential into structure determining repulsions and perturbative attractions that modify system energetics. We model this system as hard spheres of an effective diameter d ($= \int_0^\sigma dr[1 - e^{-\phi(r)}]$) and include attractions as a mean-field perturbation whose magnitude is determined from the effective hard-sphere system structure and the interaction potential. To first order, the resultant free energy is

$$F(\rho) = F_0(\rho, d) + 2\pi N \rho \beta^{-1} \int_\sigma^\infty dr\, g_0(r, \rho, d)\phi(r)r^2,$$
(31)

where the subscript 0 represents the properties of the effective hard-sphere fluid and g is the radial distribution function [23]. We express this in the language of density-functional theory by dividing the excess free energy into a hard-sphere and an attractive term

$$F[\rho] = F_{\mathrm{id}}[\rho] + F_{\mathrm{ex}}^{HS}[\rho] + F_{\mathrm{ex}}^{\mathrm{att}}[\rho]$$
(32)

now with

$$F_{\mathrm{ex}}^{\mathrm{att}}[\rho] = F_{\mathrm{ex}}^{\mathrm{att}}(\rho)$$

$$= 2\pi N \rho \beta^{-1} \int_\sigma^\infty dr'\, g_0(r'; \rho; d)\phi(r')r'^2.$$
(33)

We now extend this theory to the interface by expressing the excess attractive free energy in differential form in terms of the z-dependent "bulk" density $\rho(z)$,

$$dF_{\mathrm{ex}}^{\mathrm{att}}(z) = 2\pi d N(z)\rho(z)\beta^{-1}$$
$$\times \int_\sigma^\infty dr'\, g_0(r'; \rho(z); d)\phi(r')r'^2.$$
(34)

The free energy can now be written as the integral over infinitesimal planar slices determined by reexpressing

$dN(z)$ in terms of the planar-averaged density [$dN(z) = A\hat{\rho}(z)dz$],

$$F_{\mathrm{ex}}^{\mathrm{att}}[\rho] = \int dF_{\mathrm{ex}}^{\mathrm{att}}[\rho]$$

$$= 2\pi A \beta^{-1} \int dz \hat{\rho}(z)\rho(z)$$

$$\times \int_\sigma^\infty dr'\, g_0(r'; \rho(z); d)\phi(r')r'^2.$$
(35)

After defining

$$f_{\mathrm{ex}}^{\mathrm{att}}(z) \equiv 2\pi \rho(z) \int_\sigma^\infty dr'\, g_0(r'; \rho(z); d)\phi(r')r'^2,$$
(36)

the attractive contribution is readily incorporated into the interface model allowing us to express the interfacial tension as

$$\beta\gamma = \frac{\beta \Delta\Omega}{A}\bigg|_{\min}$$

$$= \int_{\Delta z} dz\{\hat{\rho}(z)[\beta\psi_0(\overline{\rho}(z)) + f_{\mathrm{ex}}^{\mathrm{att}}(z) - \hat{\mu}]$$

$$+ \hat{f}_{\mathrm{id}}(z) + \beta P\}.$$
(37)

The similarity between the hard-sphere energies, phase boundaries, and localization parameters computed from the MWDA and the PWDA allows us to exploit the inherent computational savings of the MWDA in our calculations of Lennard-Jones bulk solid properties. To simplify calculation for low-density fluids, we express the Lennard-Jones potential as a sum of Yukawa terms [24]
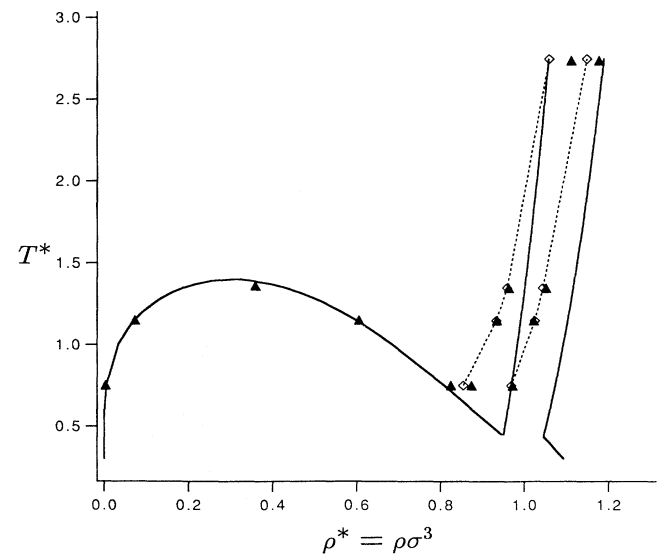

FIG. 3. Phase diagram for the Lennard-Jones fluid (——) compared to Monte Carlo simulation $\triangle$ [32] and the phase diagram predicted by Curtin and Ashcroft (-- $\diamond$ --) [25].
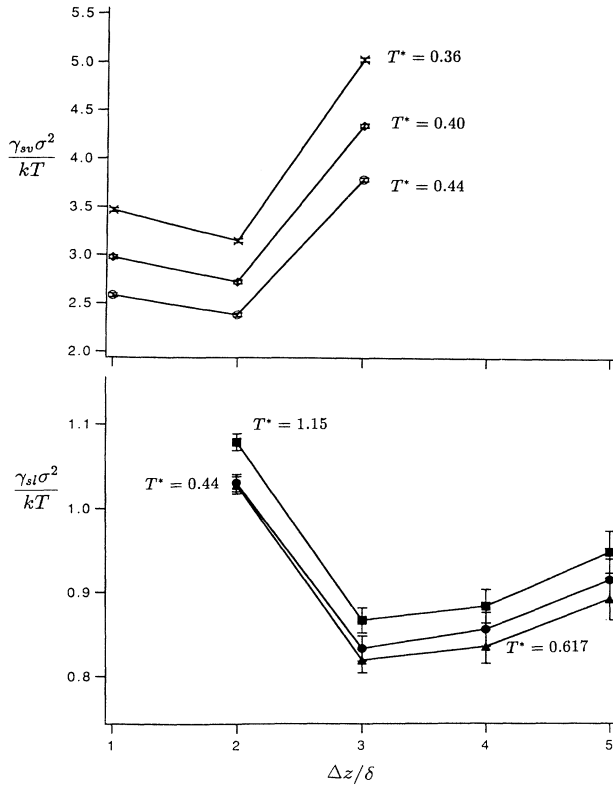
FIG. 4. Calculated interfacial tensions vs interfacial width for both the solid-liquid and solid-vapor interface (note the change in scale).

$$\phi_{lj}(r) = \frac{E}{T^*r}[e^{-a(x-1)} - e^{-b(x-1)}], \tag{38}$$

where $a = 14.735$, $b = 2.6793$, $E = 2.0199$, and $x = r/\sigma$. In addition, we approximate the solid hard-sphere radial distribution function with that for a liquid at an equivalent bulk density, which allows for a smooth transition in our treatment of the attractive contribution as we move across the phase boundary in interfacial systems. Using this approach we have computed the phase diagram shown in Fig. 3.

Having determined bulk properties μ, P, and the solid localization parameter α, we assume an interfacial width and appeal to the PWDA to determine the interfacial

weighted densities and their associated free energies. We then calculate $\hat{f}_{ex}^{att}(z)$ and $\hat{f}_{id}(z)$ for this interfacial profile and determine the interfacial tension using Eq. (37). By minimizing with respect to the interfacial width we determine simultaneously the equilibrium structure and tension of the interface. It must be noted that in the case of very low fluid densities, the value of the Fourier decay parameter ν must be set equal to zero to avoid negative local interfacial densities. We show results of these calculations in Fig. 4 and summarize the interfacial tensions in Table II.

V. DISCUSSION

The ability of this rather simple approach to describe the bulk properties of the Lennard-Jones (LJ) fluid is demonstrated in Fig. 3 when the phase diagram is compared with Monte Carlo simulation and the higher-order perturbation theory approach of Curtin and Ashcroft [25]. We use Barker-Henderson first-order perturbation theory [Eq. (31)] to accurately predict fluid properties as shown by the excellent agreement of the vapor-liquid transition at low T^*. The solid-liquid phase boundary, however, is shifted to somewhat higher densities due to the simplifying assumptions in the solid radial distribution function determining the attractive perturbation to the solid free energy, an approximation best applied to short-range potentials. Despite this shift in the phase diagram, the fractional density change upon freezing compares well to simulation as T^* is lowered and the triple point approached. As we discuss below, the interfacial tension appears to reflect the interfacial structure and thus depends on the densities of the two phases. Therefore we believe that this density difference will be the dominant influence on γ and the shift in the absolute position of the phase boundary will have a secondary effect on the results.

It is worthwhile to point out another possible approach to the determination of the Lennard-Jones free energies. de Kuijper et al. [13] have used the MWDA to determine bulk properties of LJ fluids via the direct determination of the direct correlation function. Using the HMSA [26], a combination of the hypernetted chain and mean spherical approximation closures, they solved the Ornstein-Zernike equation at a particular T^*, determined $c(r)$, and then incorporated it into the MWDA to determine the excess free energy. Unfortunately, they could not find

TABLE II. Calculated interfacial tensions for the Lennard-Jones solid-liquid (SL) and solid-vapor (SV) systems compared to the triple-point molecular-dynamics results of Broughton and Gilmer [27].

T^*	Transition	Interface width $\Delta z/\delta$	Fluid density $\rho_f\sigma^3$	Solid density $\rho_s\sigma^3$	Density difference $\Delta\rho\sigma^3$	Interfacial tension $\gamma\sigma^2/kT$	$\gamma\sigma^2/\varepsilon$
1.15	SL	3–4	0.992	1.104	0.112	0.87 ± 0.02	1.00 ± 0.02
0.617	SL	3–4	0.962	1.063	0.101	0.82 ± 0.02	0.51 ± 0.01
0.44	SL	3–4	0.950	1.046	0.096	0.83 ± 0.02	0.37 ± 0.01
0.44	SV	2	1.7×10^{-5}	1.046	1.046	2.38 ± 0.01	1.05 ± 0.01
0.40	SV	2	3.6×10^{-6}	1.060	1.060	2.72 ± 0.01	1.09 ± 0.01
0.36	SV	2	5.1×10^{-7}	1.073	1.073	3.15 ± 0.01	1.13 ± 0.01
0.617 MD	SL	~ 5–6	0.834	0.947	0.113	0.57	0.35
0.666 Curtin [12]	SL	3–4	0.882	1.015	0.133	0.65	0.43

solutions to the MWDA at temperatures $T^* < 5.0$. To overcome these difficulties, they used perturbation theory and dealt with the attractions in a mean-field fashion. This approach provided good agreement with simulation. This study demonstrates the utility of perturbation theory in describing low-temperature Lennard-Jones solids and the limitations of the MWDA in describing long-ranged interaction potentials such as the Lennard-Jones. These limitations will naturally apply to the PWDA and its ability to describe the interfacial phenomena of simple fluids.

Looking initially at the solid-liquid boundary of the phase diagram we see little variation in the magnitude of the interfacial tension $\gamma \sigma^2 / kT$ as we vary the strength of the interaction ε (see Table II). The variation we do see corresponds to the small stuctural changes induced by the decreasing density difference between coexisting phases as we lower temperature. This indicates a small *direct* influence of attractions on the interfacial tension but a large *indirect* influence in those regions of the phase boundary where small variations in interaction energy lead to very large structural changes. For this reason it is sensible to compare interfacial tensions normalized on the temperature kT rather than the strength of the attraction ε.

The influence of structure on the interfacial tension is dramatically shown as we lower the temperature below the triple point where the coexisting density difference grows tremendously, reflecting the transition from solid-liquid to solid-vapor coexistence. This transition is accompanied by a threefold increase in the calculated surface tension. In addition to the increase in the magnitude of the surface tension, solid-vapor systems show different dependence on the interaction parameter. In the solid-liquid systems, we see little change in the interfacial properties with the strength of the interaction. Below the triple point, however, small changes in ε cause significant increases in the interfacial tension as shown by the leap from $\gamma \sigma^2 / kT = 2.38 \pm 0.01$ at $T^* = 0.44$ to $\gamma \sigma^2 / kT = 3.15 \pm 0.01$ at $T^* = 0.36$. This decrease in the temperature and corresponding large increase in surface tension is accompanied by a relatively small increase in the coexisiting density difference from 1.046 to 1.073. This arises from the high energetic cost of adding mass to the solid-vapor interface resulting in a narrowing of the interface. We find a width of 2 lattice planes for the solid-vapor interface and 3-4 lattice planes for the solid-fluid interface, reflecting the weak dependence of γ on Δz in the solid-fluid case. This compares well to Curtin [12] who found that the LJ interfacial width is little changed from the hard-sphere interface value of 3-4 lattice planes.

We now compare our calculated values of the surface tension to the molecular dynamics result of Broughton and Gilmer [27]. They performed simulations of Lennard-Jones systems at their triple-point conditions ($T^* = 0.617$), determining a solid-fluid interfacial tension of $\gamma \sigma^2 / \varepsilon = 0.35 \pm 0.02$. Using our method under our triple-point conditions ($T^* = 0.44$) we calculate a value of 0.37 ± 0.01. This agreement, however, is somewhat fortuitous. Comparing the interfaces at $T^* = 0.617$ shows that

our $\gamma^{\text{PWDA}} \sigma^2 / kT = 0.82 \pm 0.02$ exceeds the molecular-dynamics (MD) result $\gamma^{\text{MD}} \sigma^2 / kT = 0.57 \pm 0.03$, while Curtin estimates a value of $\gamma^{\text{WDA}} \sigma^2 / kT = 0.65$ at $T^* = 0.666$. Though we overestimate the molecular-dynamics results, agreement is quite good considering the difficulty in determining such interfacial properties.

The Lennard-Jones system provides a rigorous test of this model because of its long range. One reason for the discrepancy in our results for the Lennard-Jones system is the fact that the long tail in the potential extends beyond neighboring layers in ordered regions. We therefore expect higher precision and better results in systems with shorter-ranged interactions. We are currently applying density-functional theory and the PWDA to the study of phase transitions induced by the addition of nonadsorbing polymer in colloidal systems. The interaction potential in these systems is of finite range and has been previously studied using perturbation theory [28] making it an ideal experimental system for study using our approach. We are confident that we are now able to study the interfacial properties of any system whose interaction potential is well characterized and amenable to study via perturbation theory.

VI. SUMMARY

We have introduced a formulation of the weighted-density approximation ideal for the study of the planar interface. This model lowers computational requirements over the original WDA giving nearly equivalent results for both hard-sphere bulk and interfacial properties. We then extend the model to simple fluids whose interactions can be described by the Lennard-Jones potential and treated via perturbation theory. We probe the influence of interaction strength on the properties of both solid-liquid and solid-vapor interfaces through the interfacial width and tension. Interaction strength has little influence on interfacial properties until the temperature is reduced beneath the triple point where we see both a narrowing of the interface and a large growth in the magnitude of γ.

ACKNOWLEDGMENTS

APPENDIX A: THE WEIGHTED DENSITY

The planar weighted-density requires a self-consistent solution of the following:

$$\overline{\rho}(z) = \rho_l + (\rho_s - \rho_l)\frac{1}{2\pi}\int dk\, e^{ikz} w(k;\overline{\rho}(z)) f_0(-k)$$

$$+ \frac{\rho_l + (\rho_s - \rho_l)f_0(z)}{2\pi\hat{\rho}(z)}\int dk\, w(k;\overline{\rho}(z)) e^{ikz}\sum_{\mathbf{G}} \delta_{G_{||},0}\rho_G f_G(k+G_z)$$

$$+ \frac{1}{2\pi\hat{\rho}(z)}\int dk\sum_{\mathbf{G}_i}\rho_{G_i} f_{G_i}(z) e^{i(G_{iz}-k)z}\sum_{\mathbf{G}_j}\delta_{G_{i||},-G_{j||}}\rho_{G_j} w((G_{j||}^2+k^2)^{1/2};\overline{\rho}(z)) f_{G_j}(k+G_{jz}) \qquad (A1)$$

where $\mathbf{G}_{||} = (G_x, G_y)$. Though this equation appears quite complex, the δ functions in the second and third terms evaluate to zero for most of the reciprocal lattice vectors used in the summation. In addition, we take advantage of lattice symmetry by recognizing that for each $(\mathbf{G}_{||}, G_z)$ there is a $(-\mathbf{G}_{||}, -G_z)$ and each magnitude $G_{||}$ has a particular set of $\{G_z\}$ associated with it. We may now reexpress the last term as

$$\frac{1}{2\pi\hat{\rho}(z)}\int dk\sum_{G_{i||}}\sum_{\{G_{i||}\}} w((G_{i||}^2+k^2)^{1/2};\overline{\rho}(z))$$

$$\times \left\{\sum_{G_{iz}} f_{G_i}(z)\rho_{G_i}\left[(1+\delta_{\{G_{i||}\},0})\cos(G_{iz}z)\cos(kz)\sum_{G_{jz}}\rho_{G_\xi}[f_{G_\xi}(k+G_{jz})+f_{G_\xi}(k-G_{jz})]\right.\right.$$

$$\left.\left. - (1-\delta_{\{G_{i||}\},0})\sin(G_{iz}z)\sin(kz)\sum_{G_{jz}}\rho_{G_\xi}[f_{G_\xi}(k+G_{jz})-f_{G_\xi}(k-G_{jz})]\right]\right\}, \qquad (A2)$$

where $G_\xi^2 = G_{i||}^2 + G_{jz}^2$. The summations over G_z are over those magnitudes associated with a particular magnitude of $G_{||}$. The sum over $\{G_{||}\}$ is over all magnitudes $G_{||}$ and the sum over $G_{||}$ is over the degeneracies of these magnitudes. Though this equation remains complex, we must remember that the weighted density must only be evaluated as one translates along in z and is not a function of x and y. Notice also that the summations over G_{jz} are z independent and need not be recalculated as one moves through the interface.

The planar-averaged crystal (see Fig. 5), like the regular three-dimensional crystal, is characterized by regions of very high and very low "local" densities. Those positions where the density approaches zero cause difficulty
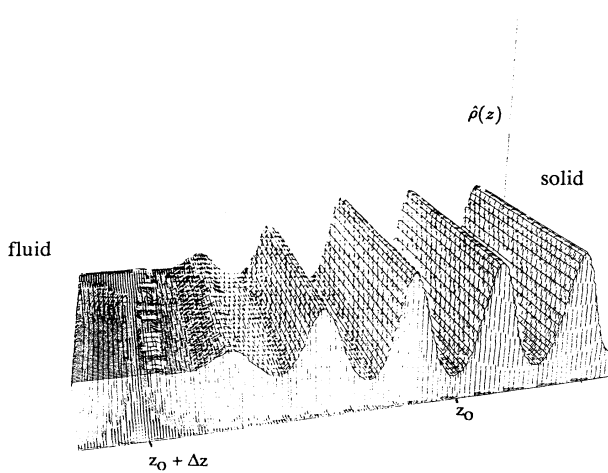
in the determination of the weighted density due to its normalization by $\hat{\rho}(z)$; however $\overline{\rho}(z)$ remains finite. The contribution to the total excess free energy $\hat{\rho}(z)\psi_0(\overline{\rho}(z))$ is also small allowing one to neglect, in practice, calculation of $\overline{\rho}(z)$ for small values of $\hat{\rho}(z)$ [taken to be $\hat{\rho}_c(z)$ = 0.01]. Figure 6 shows $\hat{\rho}(z)\psi_0(\overline{\rho}(z))$, $\hat{\rho}(z)$, and $\overline{\rho}(z)$ through one lattice plane.

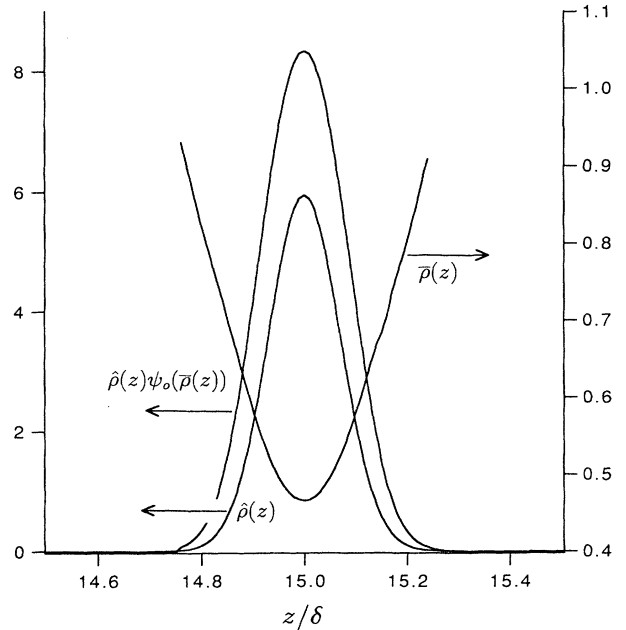FIG. 5. Planar averaged interfacial profile for the same parameters as in Fig. 1.

FIG. 6. The weighted density $\overline{\rho}(z)$, the planar-averaged density $\hat{\rho}(z)$, and the local contribution to the excess free energy $\hat{\rho}(z)\psi_0(\overline{\rho}(z))$ for hard spheres with $\rho_s\sigma^3$ = 1.026, $\rho_l\sigma^3$ = 0.882, and $\alpha\sigma^2$ = 120.0 (z_0/δ = 15.5).

APPENDIX B: ERROR ANALYSIS

We are interested in estimating the error in our computations of the interfacial tension,

$$\beta\gamma = \frac{\beta\Delta\Omega}{A}\bigg|_{\min}$$

$$= \int_L dz\{\hat{\rho}(z)[\beta\psi_0(\overline{\rho}(z)) + f_{ex}^{att}(z) - \hat{\mu}]$$

$$+ \hat{f}_{id}(z) + \beta P\}. \tag{B1}$$

Neglecting any numerical error involved in the minimization of the interfacial energy, we express $\Delta\gamma$ in terms of the individual errors

$$\Delta\gamma = \Delta\overline{\rho}\frac{\partial\gamma}{\partial\overline{\rho}}\bigg|_{\hat{\mu},P,f_{ex}^{att}} + \Delta\hat{\mu}\frac{\partial\gamma}{\partial\hat{\mu}}\bigg|_{\overline{\rho},P,f_{ex}^{att}}$$

$$+ \Delta P\frac{\partial\gamma}{\partial P}\bigg|_{\overline{\rho},\hat{\mu},f_{ex}^{att}} + \Delta f_{ex}^{att}\frac{\partial\gamma}{\partial f_{ex}^{att}}\bigg|_{\overline{\rho},\hat{\mu},P}. \tag{B2}$$

As an example we show how the error in the weighted density propagates:

$$\frac{\partial\gamma}{\partial\overline{\rho}}\bigg|_{\hat{\mu},P,f_{ex}^{att}} \approx \frac{\partial}{\partial\overline{\rho}}\int dz\hat{\rho}(z)\psi_0(\overline{\rho}(z))$$

$$\approx \int dz\,\hat{\rho}(z)\frac{\partial\psi_0(\rho)}{\partial\rho}\bigg|_{\overline{\rho}}$$

$$\approx \psi_0'(\rho_s)\int dz\,\hat{\rho}(z) \quad \text{(in the worst case)}$$

$$= \psi_0'(\rho_s)L\rho_{av},$$

where L is the interfacial width and ρ_{av} the average of the two asymptotic densities. Similarly,

$$\beta\frac{\partial\gamma}{\partial\hat{\mu}}\bigg|_{\overline{\rho},P,f_{ex}^{att}} = \beta\frac{\partial\gamma}{\partial f_{ex}^{att}}\bigg|_{\overline{\rho},\hat{\mu},P} = \rho_{av}\frac{\partial\gamma}{\partial P}\bigg|_{\overline{\rho},\hat{\mu},f_{ex}^{att}} = L\rho_{av}$$

$$\tag{B3}$$

leading to

$$\beta\Delta\gamma \approx L\left\{\rho_{av}[\beta\psi_0'(\rho_s)\Delta\overline{\rho} + \Delta\hat{\mu} + \Delta f_{ex}^{att}] + \beta\Delta P\right\}. \tag{B4}$$

TABLE III. Calculated pressures at $T^* = 1.15$ compared to the molecular-dynamics results of Hansen and Verlet [32].

ρ	$\beta P_f^{MD}/\rho$	$\beta P_s^{MD}/\rho$	$\beta P_f^{PWDA}/\rho$	$\beta P_s^{PWDA}/\rho$
0.65	0.306		0.357	
0.75	1.165		1.269	
0.85	2.860		2.933	
0.92	4.723		4.778	
1.00		4.07		3.81
1.05		6.05		4.88

For hard spheres $\rho_s = 1.026$ and $\rho_l = 0.882$; therefore, $\rho_{av} = 0.954$, $\beta\psi_0'(1.026) \approx 15$. The accuracy in our numerical calculations are $\Delta\hat{\mu} = 0.001$, $\beta\Delta P = 0.001$, $\Delta\overline{\rho} = 0.0002$, and for hard spheres $\Delta f_{ex}^{att} = 0$. Therefore

$$\beta\Delta\gamma \approx L\{0.954[15.0(0.0002) + 0.001] + 0.0 + 0.001\}$$

$$= L(0.005)$$

A typical interfacial width is 4, leading to an estimated average error of $\beta\Delta\gamma_{av} \approx 0.02$.

To estimate the error for the Lennard-Jones interfacial tension we must concern ourselves not only with the computational error associated with the integration in f_{ex}^{att} (which is quite small), but also with error in our approximation for the solid structure and the truncation in the free-energy expansion. We can compare calculated results for the pressure with those determined by the molecular-dynamics simulations of Lennard-Jones fluids by Hansen and Verlet [32] (see Table III).

As expected, we see good agreement with the calculated fluid pressures, even at high densities. Solid pressures, however, are underpredicted leading to the shift in coexistence in the phase diagram. Unfortunately, we cannot predict how these errors in the pressure will be reflected in the interfacial tension; however, it would appear from our calculations that γ is not directly dependent on the pressure but rather on the difference between the predicted coexisting densities.

[1] W.G. Hoover, B.J. Alder, and D.A. Young, J. Chem. Phys. **49**, 3688 (1968).

[2] W.G. Hoover and F.H. Ree, J. Chem. Phys. **49**, 3609 (1968).

[3] M. Baus, J. Phys.: Condensed Matter **2**, 2111 (1990).

[4] Y. Singh, Phys. Rep. **207**, 351 (1991)

[5] D.W. Oxtoby, in *Liquids, Freezing, and the Glass Transition*, Les Houches Session 51, edited by J.P. Hansen, D. Levesque, and J. Zinn-Justin (Elsevier, New York, 1990).

[6] R. Evans, in *Liquids at Interfaces*, Les Houches Session 48, edited by J. Charvolin, J.F. Joanny, and J. Zinn-Justin (Elsevier, New York, 1989).

[7] J.F. Lutsko and M. Baus, Phys. Rev. A **41**, 6647 (1990).

[8] J.F. Lutsko, Phys. Rev. A **43**, 4124 (1991).

[9] W.A. Curtin and N.W. Ashcroft, Phys. Rev. A **32**, 2909 (1985).

[10] A.R. Denton and N.W. Ashcroft, Phys. Rev. A **39**, 4701 (1989).

[11] W.A. Curtin, Phys. Rev. Lett. **59**, 1228 (1987).

[12] W.A. Curtin, Phys. Rev. B **39**, 6775 (1989).

[13] A. deKuijper, W.L. Vos, J.L. Barrat, J.P. Hansen, and J.A. Schouten, J. Chem. Phys. **93**, 5187 (1990).

[14] A. Kyrlidis and R.A. Brown, Phys. Rev. A **44**, 8141 (1991).

[15] Y. Rosenfeld, Phys. Rev. A **43**, 5424 (1991).

[16] D.M. Kroll and B.B. Laird, Phys. Rev. A **42**, 4806 (1990).

[17] B.B. Laird and D.M. Kroll, Phys. Rev. A **42**, 4810 (1990).

[18] E. Kierlik and M.L. Rosinberg, Phys. Rev. A **42**, 3382 (1990).

[19] E. Kierlik and M.L. Rosinberg, Phys. Rev. A **44**, 5025 (1991).

[20] A.R. Denton and N.W. Ashcroft, Phys. Rev. A **44**, 8242

(1991).

[21] P. Tarazona, Mol. Phys. **52**, 81 (1984).

[22] J.A. Barker and D. Henderson, J. Chem. Phys. **47**, 4714 (1967).

[23] D. Henderson, J. Colloid Interface Sci. **121**, 486 (1988).

[24] S.M. Foiles and N.W. Ashcroft, J. Chem. Phys. **75**, 3594 (1981).

[25] W.A. Curtin and N.W. Ashcroft, Phys. Rev. Lett. **56**, 2775 (1986).

[26] G. Zerah and J.P. Hansen, J. Chem. Phys. **84**, 2336 (1986).

[27] J.Q. Broughton and G.H. Gilmer, J. Chem. Phys. **84**, 5759 (1986).

[28] A.P. Gast, C.K. Hall, and W.B. Russel, J. Colloid Interface Sci. **96**, 251 (1983).

[29] J.F. Lutsko and M. Baus, Phys. Rev. Lett. **64**, 761 (1990).

[30] M. Baus and J.L. Colot, Mol. Phys. **55**, 653 (1985).

[31] A.R. Denton and N.W. Ashcroft, Phys. Rev. A **42**, 7312 (1990).

[32] J.P. Hansen and L. Verlet, Phys. Rev. **184**, 151 (1969).